atoms

IMPACT FACTOR 1.7

CITESCORE 2.7

Article

Application of Atomic Spectroscopy of Trapped Radioactive Ions in Nuclear Physics

Ruben P. de Groote

Special Issue

Advances in Ion Trapping of Radioactive Ions

Edited by

Dr. Maxime Brodeur

MDPI

https://doi.org/10.3390/atoms12120060

atoms

MDPI

Article

Application of Atomic Spectroscopy of Trapped Radioactive Ions in Nuclear Physics

Ruben P. de Groote

Instituut voor Kern-en Stralingsfysica, KU Leuven, B-3001 Leuven, Belgium; ruben.degroote@kuleuven.be

Abstract: A review is given of precision measurements of hyperfine constants and nuclear g-factors measured with ions confined in ion traps. The nuclear physics observables which can be extracted from these types of measurements are discussed. The feasibility of future nuclear structure studies using precision atomic spectroscopy of trapped radioactive atoms, produced with accelerator-driven approaches, is discussed.

Keywords: nuclear physics; electromagnetic moments; g-factors; ion traps; laser spectroscopy; double-resonance

Citation: de Groote, R.P. Application of Atomic Spectroscopy of Trapped Radioactive Ions in Nuclear Physics. *Atoms* **2024**, *12*, 60. https://doi.org/10.3390/atoms12120060

Academic Editor: Maxime Brodeur

Received: 30 August 2024
Revised: 13 November 2024
Accepted: 19 November 2024
Published: 21 November 2024

1. Introductory Concepts

Ion traps have become a ubiquitous tool in modern physics research due to their ability to confine ions for a long time in a vacuum, which enables high-fidelity manipulation of their motional and internal state. By combining atom or ion traps with suitable laser systems and/or radiofrequency fields, highly precise spectroscopy is made possible. In particular, nuclear g-factors and atomic hyperfine structure can be measured with high accuracy [1], which informs us on the structure of the underlying nucleus. Recently, progress in atomic isotope shift measurements has also provided insight into nuclear shape and size [2]. Despite ample demonstration of the small number of ions which are required for such precision measurements, studies have predominantly been focused on only the study and manipulation of stable isotopes—indeed, radioactive isotopes have essentially not been studied. Of the few exceptions, some focus on long-lived isotopes in an offline context [3–6], though a few online studies of short-lived isotopes (Be [7–9] and Ra [10]) have been performed. This paper aims to examine the potential and feasibility of future measurements with trapped, short-lived radioactive ions. To do so, an updated survey of the current literature and state-of-the-art is performed, building on earlier reviews and reference texts [1,11–13]. Note that the scope of this paper restricts itself to the study of singly-charged ions, despite many impressive and interesting measurements using trapped neutral atoms (even radioactive ones [14–16]), as well as highly charged ions [17]. This survey provides the background and context to motivate planned experiments with radioactive isotopes. This paper is thus structured as follows. In Section 1, a brief description of some essential concepts is given: the operational principles behind Penning and Paul traps, nuclear- and atomic g-factors, and atomic hyperfine structure. A survey of precision measurements performed on these effects using ion traps is then presented, highlighting particular examples in Section 2. Finally, the paper concludes with an outlook towards future measurements using short-lived atoms.

1.1. Atomic and Nuclear Structure

Atomic nuclei are composed of nucleons, protons and neutrons, which can be thought of as occupying different nuclear orbitals. The orbital motion of these nucleons, combined with their intrinsic spin, can impart a net non-zero nuclear spin I and magnetic moments onto the nucleus. This nuclear spin I is obtained by summing the orbital and spin angular

momenta of all the nucleons. Due to pairing, all nuclei with an even number of protons and neutrons have a ground-state total spin of zero and, thus, also no measurable electromagnetic moments. The shape of the distribution of the protons does not have to be spherical, and in fact rarely is, which gives rise to non-zero electrical multipole moments. The presence of these electromagnetic moments gives rise to a perturbation of the energies of bound electrons, called hyperfine structure. This hyperfine structure is present for all atomic systems where J, the sum of all angular momenta of the electrons, is larger than zero.

The energies of the same atomic state are also observed to differ between isotopes of the same element. This effect is called the isotope shift, and is due in part to the changing mass of the nucleus, and in part due to the change in the size of the nuclear charge distribution. Recently, there has been a flurry of activity in precision isotope shift studies, mainly motivated by searches for physics beyond the standard model. Intriguingly, these searches have so far provided insight into not just the commonly measured nuclear mean-squared charge radius $\delta\langle r^2\rangle$, but also the next radial moment $\delta\langle r^4\rangle$ [2,18]. Extending such measurements to radioactive isotopes would provide a handle on the surface thickness of nuclear density [19]. An exploration of perspectives of this new avenue of research is outside of the scope of this work, which instead focuses on precision hyperfine structure measurements.

1.1.1. Hyperfine Structure

We define the total angular momentum of an atom as $\vec{F}$, where $\vec{F} = \vec{I} + \vec{J}$, with $\vec{J}$ representing the total angular momentum of the atomic state. From angular momentum addition rules, it follows that F can assume values in the range $|I-J|, |I-J|+1, \ldots I+J$. Using first-order perturbation theory, the energy shift of a state with total angular momentum F due to the hyperfine interaction between the nucleus and electron can then be written as [20]:

$$E_F^{(1)} = \sum_k M_k(I,J,F)\langle II|T_k^{(n)}|II\rangle\langle JJ|T_k^{(e)}|JJ\rangle, \tag{1}$$

where

$$M_k(I,J,F) = (-1)^{I+J+F}\frac{\begin{Bmatrix} I & J & F \\ J & I & k \end{Bmatrix}}{\begin{pmatrix} I & k & I \\ -I & 0 & I \end{pmatrix}\begin{pmatrix} J & k & J \\ -J & 0 & J \end{pmatrix}}.$$

The hyperfine interaction lifts the degeneracy of the hyperfine levels, with the energy shifts in this multiple expansion decreasing as the multipole order increases. Defining $K = F(F+1) - I(I+1) - J(J+1)$, this can be written as follows (truncated at the octupole ($k=3$) term):

$$\begin{aligned} E_F^{(1)} = {} & \frac{AK}{2} + B\frac{3}{4}\frac{K(K+1) - I(I+1)J(J+1)}{(2I(2I-1)J(2J-1))} \\ & + \frac{5C}{4}\frac{K^3 + 4K^2 + \frac{4}{5}K(-3I(I+1)J(J+1) + I(I+1) + J(J+1) + 3) - 4I(I+1)J(J+1)}{I(I-1)(2I-1)J(J-1)(2J-1))} \\ & + D\ldots, \end{aligned} \tag{2}$$

with hyperfine constants

$$\begin{aligned} A &= \tfrac{1}{IJ}\langle II|T_2^{(n)}|II\rangle\langle JJ|T_1^{(e)}|JJ\rangle &&= \frac{\mu_I}{IJ}\langle JJ|T_1^{(e)}|JJ\rangle \\ B &= 4\langle II|T_2^{(n)}|II\rangle\langle JJ|T_2^{(e)}|JJ\rangle &&= 2eQ\langle JJ|T_2^{(e)}|JJ\rangle \\ C &= \langle II|T_3^{(n)}|II\rangle\langle JJ|T_3^{(e)}|JJ\rangle &&= -\Omega\langle JJ|T_3^{(e)}|JJ\rangle. \\ D &= \langle II|T_4^{(n)}|II\rangle\langle JJ|T_4^{(e)}|JJ\rangle &&= \Pi\langle JJ|T_4^{(e)}|JJ\rangle. \end{aligned} \tag{3}$$

These latter formulae show how each term in the multipolar expression is the product of an electronic matrix element and a nuclear moment (μ_I: magnetic dipole; Q: electric quadrupole; Ω: magnetic octupole; Π: electric hexadecapole). These moments are the quantities of interest for nuclear structure studies, while the former can either be calculated, or extracted by combining hyperfine structure measurements with other independent measurements of the nuclear moments. Typical orders of magnitude of frequency shifts due the different multipole orders vary strongly depending on the atomic levels which are studied. While the dipole and quadrupole contributions are typically in the order of 100 MHz–GHz, octupolar shifts are usually 1 kHz or less [21]. Accurate extraction of this moment from hyperfine structure data requires extending the above analysis to the second-order perturbations (where, again, atomic matrix elements need to be computed or otherwise determined), which can be of the same order of magnitude or larger [20,21].

In addition to this hyperfine structure, the non-zero magnetic moment of the nucleus also gives rise to a Zeeman shift when the atom is placed in a magnetic field. The Zeeman shift of a state with angular momentum F and projection quantum number m_F is, in the low-field limit, given in the first order by

$$E_{m_F}^{(1)} = \mu_B B_{\text{ext}} m_F \left(g_J \frac{F(F+1) - I(I+1) + J(J+1)}{2F(F+1)} + \frac{\mu_N}{\mu_B} g_I \frac{F(F+1) + I(I+1) - J(J+1)}{2F(F+1)} \right) \tag{4}$$

Typical values are in the order of 10 MHz/mT. The contribution of the nuclear g-factor to the total Zeeman shift is typically ∼2000 times smaller than the shift due to the magnetic moment of the electron (due to the larger mass of the nucleons, $\mu_N/\mu_B \approx 1/1837$). Thus, at low fields, high precision (better than kHz) is required to measure the contribution due to the nucleus. It can thus be advantageous to perform measurements using large magnetic fields, e.g., those generated in a Penning trap. Note that in this case, the low-field expression (4) does not hold; for very large fields, it may even be necessary to take into account mixing with close-lying fine structure levels.

There are additional effects, beyond those of Equations (1) and (4), which may need to be considered, depending on the precision of the measurements. If there are other electronic levels sufficiently close by, second-order perturbation theory may need to be invoked to yield the correct energy shifts due to the hyperfine interaction. Diamagnetic corrections may also have to be considered, to account for, e.g., changes in the electronic spin density at the nucleus induced by magnetic fields. As a consequence, measurements performed in different magnetic fields may not agree unless this diamagnetic effect is taken into account. Extracting the nuclear moments from the experimental hyperfine constants by taking the ratio with another isotope with a known moment may also require correcting for the hyperfine anomaly [22,23]. Conversely, precise measurements of the hyperfine constants of several atomic levels of a given element provide a way to measure this hyperfine anomaly, which, in turn, provides information on the distribution of nuclear magnetization (see, e.g., [16] for an example of such measurements using a Fr atom trap).

1.1.2. Nuclear Moments as Probes for Nuclear Structure

As indicated in Equation (1), measurements of hyperfine intervals provide nuclear-model-independent access to the underlying nuclear electromagnetic moments (though they may depend on atomic theory, in case no suitable reference measurement exists to

calibrate the atomic matrix elements in Equation (1)). The first two terms in the multipole expansion, the magnetic dipole and the electric quadrupole moment, have been extensively studied over the decades. These studies span nearly the entire nuclear chart, and are often performed on long isotopic chains, thanks to the efficiency and versatility of modern laser spectroscopy techniques in radioactive ion beam laboratories [24]. These two moments provide rich insight into nuclear structure and serve as good tests for nuclear theory [25,26]. The next moment, the magnetic octupole moment, has only scarcely been studied. This is mainly due to the small contribution of the magnetic octupole moment to the total hyperfine shifts. This can be seen in the compiled data provided in tables discussed later in this paper. The next term, the electric hexadecapole moment, contributes less still and has yet to be convincingly extracted [27], though plans are underway for Yb^+ [28].

1.2. Experimental Tools

1.2.1. Ion Traps

Two types of traps are commonly used to aid in the spectroscopy of charged particles: Paul traps and Penning traps. More details on their basic principles of operation can be found in, e.g., [29,30]. Below, we briefly summarize the essentials.

A Paul trap is a type of ion trap that uses dynamic electric fields to confine charged particles in a three-dimensional region of space. Oscillating electric potentials, sometimes in combination with static electric fields, are applied to a suitable set of electrodes, creating a quadrupole electric field that varies in time and space. Many different electrode geometries have been demonstrated in the literature. The stability of the motion depends on the mass-to-charge ratio of the particles, the amplitude and frequency of the oscillating potential, and the geometry of the electrodes. When filled with a buffer gas, typically helium, these devices can also be used to cool ion beams down to the temperature of the buffer gas. These cooled beams can then also be released in bunches; the timing structure that is thus imprinted on the ion beam can then be exploited by experiments placed downstream of the trap.

A Penning trap uses a quadrupole electric field and a homogeneous magnetic field, rather than oscillating electric fields. The charged particles experience a Lorentz force from the magnetic field that confines them radially and an electrostatic force from the electric field that confines them axially. The motion of the particles can be decomposed into three harmonic modes: the axial mode along the magnetic field, the magnetron mode perpendicular to the magnetic field and opposite to its direction, and the cyclotron mode perpendicular to the magnetic field and in its direction. The presence of the large and homogeneous magnetic field makes Penning traps well suited for measurements of nuclear g-factors, as will be discussed next. Penning traps have also been used extensively for precision mass measurements of stable and unstable isotopes [31,32], which provide valuable information about the nuclear structure of these atoms.

1.2.2. Optical and Optical-Radiofrequency Double Resonance Spectroscopy

The storage of ions inside ion traps enables high-resolution spectroscopy by probing the state of the ion as, e.g., an optical or rf field is tuned. For all examples of precision hyperfine structure constants and nuclear g-factors, which are discussed further in this manuscript, this state detection is achieved through the detection of photons scattered by the ions when irradiated by a (near-)resonant laser beam driving a strong optical transition. An ion which scatters photons is called *bright*, indicating that the state of the ion is one of the states involved in the laser excitation cycle, while one that does not is *dark*. It is also possible to map the state of the ion onto a dark state, a technique called electron shelving [33,34]. Other methods of state determination also exist (see, e.g., [35,36]), but are beyond the scope of this brief overview.

Irrespective of the details of the measurement scheme, fundamentally, the best achievable experimental precision is 'Fourier-limited', that is, inversely proportional to the interaction time between the probing fields and the ions $\delta\nu \sim 1/t$. This time is maximized by trapping the ions in a trap. These long interaction times also enable careful manipulation

of the internal state of the ion, and, furthermore, enable the scattering and detection of many photons per ion. This latter point is especially important for the study of radioactive isotopes: since only a few ions of interest may be available for study, it is a necessity to have as high an experimental efficiency as possible. In addition to the precision of the measurement, systematic effects also need to be considered. These will vary depending on the details of the measurement scheme and the ion trap system; in all cases, one needs to worry about the external fields (electric and magnetic) which the ion experiences, and to ensure these are well controlled and stable throughout the measurements.

Extracting the nuclear observables of interest from the measured frequencies requires additional knowledge. For nuclear g-factors, the value of the external magnetic field needs to be known at the desired level of accuracy, e.g., through measurements on reference cases or other forms of co-magnetometry. In order to obtain nuclear moments from measured hyperfine constants, one can also take ratios with other isotopes where the moment of interest is known, assuming a sufficiently accurate reference exists from, e.g., nuclear magnetic resonance methods, or by relying on atomic theory. The latter is required for magnetic octupole moments, since no reference moments obtained with non-optical methods currently exist. The accuracy of these theory calculations is not straightforward to estimate, but they are now, in principle, sufficiently accurate for the simple atomic systems most readily studied in ion traps [28,37,38].

To reach a Fourier-limited precision, optical spectroscopy using fast dipole-allowed transitions to excited states with typical lifetimes of only a few ns is not an option, as the natural width of these states is in the order of a few MHz. Two alternatives are available. The first is to drive optically forbidden transitions (quadrupole or octupole transitions). With natural widths of Hz or less, the linewidth is solely determined by three factors: the distribution of ion velocities (i.e., Doppler broadening); the bandwidth of the laser; and the interaction time between the lasers and the ions. Assuming the ions are cooled sufficiently, and a sufficiently stable and narrowband laser is used (e.g., a bandwidth of only a few tens of times the desired precision), it is the latter contribution which dominates the linewidth and which thus determines the precision. Establishing such long coherence times is, however, challenging. Precision measurements of hyperfine structure using optically forbidden lines are, however, only scarcely reported on.

A second option, used far more often for hyperfine structure studies, relies on laser-radiofrequency double-resonance techniques. Lasers are still used, but for state preparation and readout, rather than for spectroscopy. Instead, magnetic dipole transitions within a hyperfine manifold of a given fine-structure state are driven using radiofrequency photons. This method is considerably less technologically challenging, and can be traced back to early in the 20th century [39]. For this reason, it sits at the heart of (hyperfine-based) atomic clocks and has been used extensively for precision hyperfine structure measurements. Figure 1 provides an illustration of the different steps in a generic laser–double resonance experiment.

First, the ion is prepared in a desired state within the hyperfine or Zeeman manifold of interest. This can be achieved by using an optical pumping process, as illustrated in Figure 1. Alternatively, coherent population transfer can be achieved using Raman processes [40], or by using a dipole-forbidden transition [41] to selectively excite to the desired level. In the second step, the ion is irradiated by radiofrequency (rf) photons for a well-defined time. On resonance, these photons will drive the ion into a different state of the manifold. In the third step, the state of the ion is probed. In Figure 1, an example is given where the ion is irradiated with the same laser as was used for state preparation—in this case, no fluorescence will be emitted if the rf transition was successful. Repeating this process for different rf frequencies and for different initial states enables determination of the hyperfine intervals. In more sophisticated detection schemes, the state of the ion can also be mapped onto a dark state, again, using, e.g., an optical pumping process of a coherent transfer. Some ions can then be made to scatter photons nearly indefinitely. Thus, even a single ion in the trap at a time can be sufficient for spectroscopy.

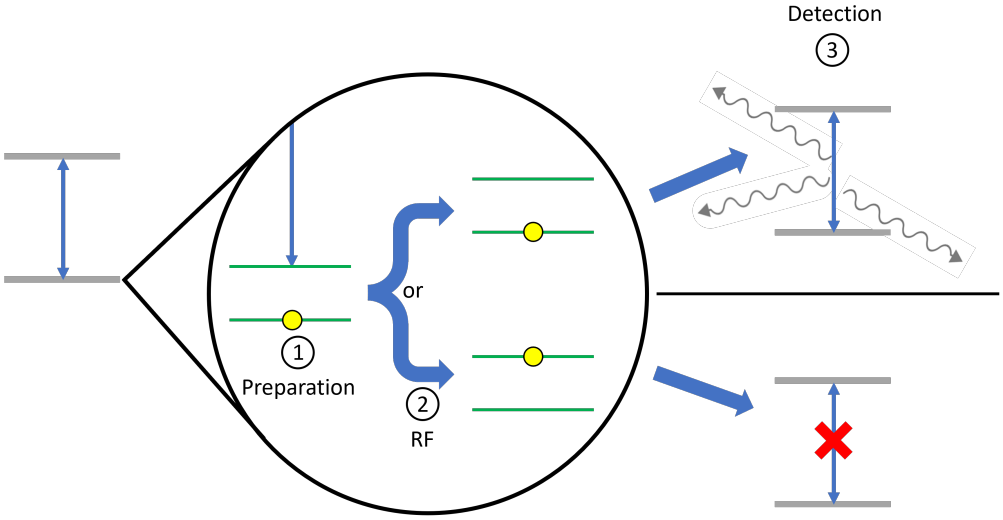

Figure 1. A diagram depicting the basic principles of laser-radiofrequency double resonance spectroscopy. By driving a transition from one of the states of the ground-state multiplet, the ion can be prepared in an initial state (step 1). In step 2, the rf field is applied, which leads to either an excitation (bottom path), or not (top path). The state of the ion is then read out in the third step, thus determining whether step 2 succeeded in changing the state of the ion.

1.2.3. Cooling of Trapped Charged Particles

The state preparation and detection steps of a laser–double resonance experiment both require the ability to selectively drive optical resonance. This can be achieved by exploiting the selection rules. For example, irradiation of the ion with resonant laser light with circular polarization along the quantization axis will eventually pump the ion into states with maximal projection quantum numbers m. When conducting hyperfine structure measurements, it is usually a requirement that the hyperfine structure can at least partially be optically resolved. Depending on the size of the hyperfine splittings, this may require cooling the ions.

Cooling trapped ions can be achieved in a few ways [42]. Ions can be cooled through collisions with buffer gas. The lowest temperature which can be achieved is limited by the temperature of the buffer gas. Importantly, this method is universal and can be applied to cool all species, provided unwanted chemical reactions of the ion of interest with the buffer gas (impurities) are avoided. Temperatures below room temperature are not strictly required for precision measurements [43], as evidenced by examples in the literature [4,27,44]. For most cases, however, resolving the hyperfine structure requires substantially lower temperatures. Temperatures in the order of mK or less can be achieved using laser cooling techniques [45]. Further cooling to the ground state of the quantum harmonic oscillator of the ion trap is also possible using, e.g., resolved sideband cooling [46], Raman sideband cooling [47], or electromagnetically induced transparency cooling [48,49]. Only a handful of elements can be laser-cooled as singly-charged ions, which is one of the drawbacks of the method (in particular when compared to buffer gas cooling). A way to circumvent this issue is to co-trap ion(s) of a different laser-coolable species, which leads to sympathetic cooling of the ion of interest [50].

2. Precision Atomic Structure Measurements with Ion Traps

Nuclear g-factors can be measured with a variety of methods; in particular, nuclear magnetic resonance (NMR) techniques are well established. Also noteworthy is the method of β-NMR, which enables measurements of the nuclear g-factor of short-lived, β-decaying nuclei. NMR methods rely on embedding the atom of interest in a solid or liquid. In contrast, the methods which are discussed in detail here confine the ions in a vacuum, thus eliminating the effects of the potentially perturbing environment of the atom. Table 1

summarizes measurements of nuclear g-factors obtained with ion trap techniques. Of particular note are the measurements on Al^+ and Ca^+ as they were obtained using Paul traps in comparatively low magnetic fields. This is in contrast to the other measurements, which used Penning traps. The Al^+ measurements are also noteworthy, since the g-factor was obtained from quantum logic spectroscopy with the electric quadrupole transition of a sympathetically cooled Al^+ ion. This illustrates the potential synergies in the developments of new optical clocks and nuclear physics-driven studies. Table 1 illustrates the high accuracy which can be achieved, but also the relatively small number of elements which have been studied. Furthermore, only one isotope has been studied in a given isotopic chain. This means that a comparison with, e.g., nuclear theory can only be carried out on the basis of *absolute* values rather than relative ones, which renders any deeper interpretation challenging.

The hyperfine constants obtained with trapped ions are summarized in Table 2; the table only reports on measurements with laser-rf techniques. Compared to nuclear g-factor measurements, more isotopes have been studied. In addition to the single-electron He, the alkaline-earth metals (Be, Mg, Ca, Sr, Ba) and alkaline-earth-like elements (Cd, Hg, Yb) make up most of the data. This can be understood from their structure: in the singly charged state, all these elements feature a single valence electron in an s-orbit, with the other electrons fully filling up the other shells. The simpler atomic structure which comes with this configuration makes these elements readily laser-coolable and simplifies state preparation and readout. Before discussing these elements in more detail, we briefly discuss the three notable exceptions: S, Eu, and Pb.

The measurements on S were performed using negative ions, the only example of this possibility which is listed in Table 1, which are confined in a Penning trap. The structure of singly-ionized S (or neutral S for that matter) is not conducive to optical spectroscopy or precision studies, so the use of a negative ion was required for precision measurements. State preparation was achieved by exploiting the polarization dependence of the photo-detachment process (which neutralizes the negative ion). This photo-detachment is also used in the detection step, after the radiofrequency excitation among hyperfine sub-levels has taken place: the number of ions remaining in the trap is measured as a function of the rf frequency.

For Pb, buffer gas cooling provided sufficiently cold ions for state preparation and readout with an optical magnetic dipole transition. This was possible despite it being a weak transition, thanks to the long laser–atom interaction time (2 s) afforded by using ion traps with a long storage time (several weeks). Isotopically pure samples were used.

The Eu measurements report on the most complex atomic structure of Table 2. The structure of the Eu^+ ion features several long-lived metastable states to which the excited Eu ions can decay. To maintain efficient-state optical pumping, rather than introducing a complex system of repump lasers, quenching through collisions with the N_2 buffer gas is used to bring the electrons back to the ground state to re-establish the fluorescence. The hyperfine structure of the ground state of Eu^+ is sufficiently large to be resolved even with room-temperature buffer gas cooling. Also noteworthy is that long-lived radioactive isotopes of Eu, produced at the ISOLDE laboratory in CERN and then transported to the ion trap laboratory in Mainz, could also be studied.

Most of the remaining entries in Table 2 report on the ground-state $S_{1/2}$ hyperfine A-constant, with sub-Hz (better than part-per-billion) precision. Note that for (stable) Be, Mg, Ca, and Ba, there are also very precise nuclear g-factors reported in Table 1. Extending these measurements of hyperfine constants and g-factors would provide insight into the evolution of the hyperfine anomaly throughout the nuclear chart. Furthermore, highly precise measurements of more than one atomic state also enable the extraction of this hyperfine anomaly, even if no nuclear g-factor is known [51]. This analysis was applied to the Europium isotopes, the longest chain with high-precision hyperfine constant measurements for five isotopes. From this analysis, structural features like odd–even staggering behavior, and deviations from the empirical Moskowitz–Lombardi formula, could be established.

In addition to ground-state measurements, in the past few years, experimental efforts were also made to study the hyperfine structure of metastable $D_{3/2,5/2}$ states of Ba^+. Of interest here is that this provides access to not only the hyperfine A-constant, but also the B-constant and C-constants. In particular, the hyperfine C-constant, which is proportional to the nuclear magnetic octupole moment, has only scarcely been measured (see Ref. [21] for an overview). Thanks to the use of trapped ions, the measurements of the C-constant on Ba offer by far the highest relative precision to date. These measurements require more intricate state preparation and readout procedures, which could nevertheless be applied to other elements with similar electronic structures, e.g., Ca^+, Sr^+ or Yb^+. The feasibility of studying the $^2F^0_{7/2}$ state in Yb^+ was also investigated [28], though it has not yet been pursued experimentally.

Few measurements of the magnetic octupole moment exist, and even fewer attempts at interpreting them through the lens of nuclear theory exist. The simplest possible perspective is offered by the single-particle shell model prediction, first proposed by Schmidt [52]. These work, on average, quite well for magnetic dipole moments (when including 60% quenching of the spin g-factor) [26]. However, as illustrated in Figure 2, this agreement is not observed for magnetic octupole moments. These theoretical curves were calculated using the single-particle formulae derived in [20]. In order to construct these curves, estimates of the single-particle orbit radius $\langle r^2 \rangle$ are required; these were approximated by the nuclear mean-squared charge radius $\langle r^2 \rangle$ taken from [53]. Using the same quenching factor of 0.6, which works well for magnetic dipole moments, nuclei with a valance configuration where $I = l + s$, i.e., where the spin and angular momenta are aligned, have magnetic octupole moments that are typically smaller than the predictions, whereas for cases with $I = l - s$, the opposite is true. Note also that there are very few datapoints for nuclei with an odd number of neutrons. This provides the motivation for the present paper to investigate how precision measurements in ion traps can contribute. Note that all alkaline-earth atoms, which are readily studied with high precision in ion traps, have an even number of protons. They thus form natural and ideal candidates for higher-order nuclear moment studies.

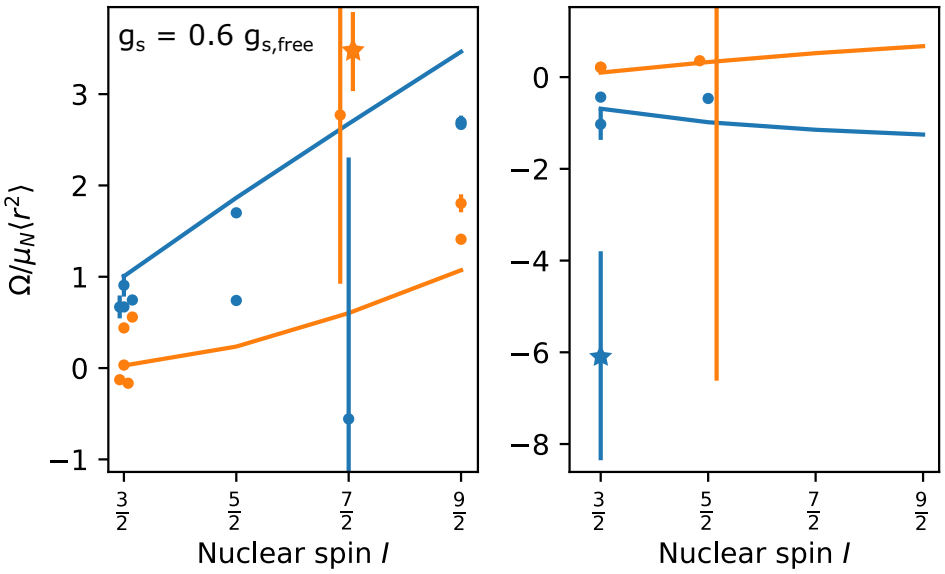

Figure 2. The experimental values of the magnetic octupole moment Ω divided by the square of the nuclear radius, in units of the nuclear magnetons μ_N, compared to single-particle estimates with an effective g_S-factor (60% quenching). The orange color indicates parallel alignment of the orbital and spin angular momenta, and the blue color anti-parallel alignment. The left panel shows odd-proton nuclei; the right panel odd-neutron nuclei. The stars indicate 'outlier' values (^{133}Cs and ^{155}Gd)), which are far larger in size than the quenched single-particle model can account for.

Table 1. Nuclear g-factors measured in ion traps. Except for $^{43}_{20}Ca^+$ and $^{27}_{13}Al^+$, all were obtained using Penning traps. * Only g_I/g_J is reported; g_I was obtained using g_J = 2.002263(6) [54]. ** The first uncertainty is due to the uncertainty on the hyperfine splitting from [55], and the second is statistical.

Isotope	I	g_I	Ref.
$^{9}_{4}Be^+$	3/2	0.823312758(25) *	[54]
		0.82331294(11) *	[56]
$^{25}_{12}Mg^+$	5/2	3.419804(27)	[57]
$^{27}_{13}Al^+$	5/2	3.64067(28)	[58]
$^{43}_{20}Ca^+$	7/2	−1.315349(9)[4] **	[59]
$^{137}_{56}Ba^+$	3/2	0.623876(3)	[60]
$^{151}_{63}Eu^+$	5/2	1.37734(6)	[61]

Table 2. The atomic hyperfine constants measured in ion traps using double-resonance methods. All measurements were performed in linear Paul traps, except for $^{9}_{4}Be^+$ and $^{25}_{12}Mg^+$, where a Penning trap was used. * The hyperfine A and B constants in [41] are not corrected for second-order HFS, and are thus not included here. The quoted uncertainty on C is purely statistical. ** The first uncertainty is due to statistical and systematic effects, and the second is the uncertainty in the frequency of the reference time standard.

Isotope	I	Atomic State	Const.	Value (Hz)	Ref.
$^{3}_{2}He^+$	1/2	$S_{1/2}$	A	8,665,649,867(10)	[62]
$^{7}_{4}Be^+$	3/2	$S_{1/2}$	A	−742,772,280(430)	[8]
$^{9}_{4}Be^+$	3/2	$S_{1/2}$	A	−625,008,837.048(10)	[54]
				−625,008,837.044(12)	[63]
$^{11}_{4}Be^+$	3/2	$S_{1/2}$	A	−2,677,302,988.8(72)	[9]
$^{25}_{12}Mg^+$	5/2	$S_{1/2}$	A	−596,254,376(54)	[57]
				−596,254,248.7(42)	[64]
$^{33}_{16}S^-$	3/2	$^2P_{3/2}$	A	91,490,000(90,000)	[65]
			B	26,240,000(230,000)	[65]
$^{43}_{20}Ca^+$	7/2	$S_{1/2}$	A	−806,402,071.60(8)	[55]
$^{87}_{38}Sr^+$	9/2	$S_{1/2}$	A	−1,000,473,673(11)	[66]
$^{111}_{48}Cd^+$	1/2	$S_{1/2}$	A	14,530,507,349.9(11)	[67]
$^{113}_{48}Cd^+$	1/2	$S_{1/2}$	A	15,199,862,858(2)	[68]
				15,199,862,855.0(2)	[69]
				15,199,862,854.96(12)	[67]
				15,199,862,855.02799(27)	[70]
$^{131}_{56}Ba^+$	1/2	$S_{1/2}$	A	9,107,913,698.97(50)	[3]
$^{133}_{56}Ba^+$	1/2	$S_{1/2}$	A	9,925,453,554.59(10)	[3]
$^{135}_{56}Ba^+$	3/2	$S_{1/2}$	A	3,591,670,117.45(29)	[71]
$^{137}_{56}Ba^+$	3/2	$S_{1/2}$	A	4,018,870,833.85(18)	[72]
		$D_{3/2}$	A	189,731,101(17)	[37]
			B	44,536,612(34)	[37]
			C	36.546(86)	[37]
				36.91(36)	[41] *
		$D_{5/2}$	A	−12,029,234(11)	[40]
			B	59,525,520(110)	[40]
			C	−12.41(77)	[40]

Table 2. *Cont.*

Isotope	I	Atomic State	Const.	Value (Hz)	Ref.
$^{148}_{63}Eu^{+}$	5	$^{9}S_{4}$	*A*	517,281,950(150)	[4]
			B	2,292,630(1000)	[4]
		$^{7}S_{3}$	*A*	−561,647,000(100,000)	[44]
$^{149}_{63}Eu^{+}$	5/2	$^{9}S_{4}$	*A*	1,585,450,570(250)	[4]
			B	534,850(1900)	[4]
$^{150}_{63}Eu^{+}$	5	$^{9}S_{4}$	*A*	599,010,680(40)	[4]
			B	−839,730(3000)	[4]
		$^{7}S_{3}$	*A*	−650,334,000(2000)	[44]
$^{151}_{63}Eu^{+}$	5/2	$^{9}S_{4}$	*A*	1,540,297,394(13)	[27]
			B	−660,862(231)	[27]
			C	26(23)	[27]
			D	−6(5)	[27]
		$^{7}S_{3}$	*A*	−1,672,457,109(266)	[44]
$^{153}_{63}Eu^{+}$	5/2	$^{9}S_{4}$	*A*	684,565,993(9)	[27]
			B	−1,752,868(84)	[27]
			C	3(7)	[27]
			D	−5(2)	[27]
		$^{7}S_{3}$	*A*	−743,183,577(82)	[44]
$^{171}_{70}Yb^{+}$	1/2	$S_{1/2}$	*A*	12,642,812,118.466(2)	[73]
				12,642,812,118.471(9)	[74]
				12,642,812,118.4682(4)	[75]
$^{173}_{70}Yb^{+}$	5/2	$S_{1/2}$	*A*	3,497,240,079.85(3)	[76]
$^{199}_{80}Hg^{+}$	1/2	$S_{1/2}$	*A*	40,507,347,997.8(10)	[77]
				40,507,347,996.9(3)	[78]
				40,507,347,996.8(1)	[78]
				40,507,347,996.84159(14)[41] **	[79]
$^{207}_{82}Pb^{+}$	1/2	$P_{1/2}$	*A*	12,968,180,601.61(22)	[80]

3. Perspectives for Nuclear Structure Studies with Trapped Radioactive Ions

Radioactive Ion Beam Production

Extending the high-precision hyperfine structure measurements on the elements which are predominantly featured in the data in Tables 1 and 2 to radioactive isotopes would significantly improve our knowledge of hyperfine anomalies and higher-order nuclear moments. Furthermore, the study of long isotopic chains would bring insight into how this nuclear moment evolves as, e.g., nuclear shell closures are crossed ($N = 20, 28$ for Ca, $N = 50$ for Sr, $N = 82$ for Ba), or how they are affected by nuclear deformation, be it quadrupole deformation (prominently present in the isotopic chains of Yb, Sr, and Ba) or even octupole deformation (present in neutron-rich isotopes of Ba and in Ra). All of this would provide a rich testing ground for nuclear theory.

In order to plan out the experimental requirements for future experiments, it is instructive to examine the typical production mechanisms and the associated radioactive isotope production rates in current-day radioactive ion beam (RIB) laboratories. In principle, all currently operational RIB laboratories (alphabetically: CARIBU inm Argonne (US), NSCL/FRIB (US), GANIL (France), GSI/FAIR (Germany), the Accelerator laboratory in Jyväskylä (Finland), ISOLDE in CERN (Switzerland), JINR (Russia), RIKEN (Japan), TRIUMF (Canada)) and planned laboratories (ISOL@Myrrha (Belgium), SPES (Italy), ...) already have or could develop the means to perform precision spectroscopy on trapped ions.

While the details vary from facility to facility, all rely on impinging an energetic particle, e.g., a fast ion beam (energies of a few 10 MeV per nucleon, or even as high as 1.4 GeV), onto a suitable target. This induces a nuclear reaction (e.g., fusion evaporation, fission, spallation, ...), which leads to the production of radioactive isotopes. Differing facilities will then have distinct ways of bringing the reaction products from the interaction

site to the user. Many laboratories have developed the ability to deliver beams with moderate energies of a few 10s of keV. At 30 keV, a nucleus with a mass of 100 mass units thus travels at a speed of 0.25 m/µs. This high velocity is required for efficient ion beam transport, and is also required for mass selection using the large dipole magnet systems in use at many facilities. This immediately implies that a precision trapping experiment at an RIB facility needs to first decelerate this beam in order to enable efficient trapping. One method is to implant and re-evaporate the radioactive atoms, as has already been carried out for long-lived isotopes of Eu [4,44]. This has the advantage of providing atoms at thermal velocities, which simplifies the next step of trapping and cooling. The downside lies in the efficiency and timescale of this process, which may prevent the study of rarer or shorter-lived isotopes. Alternatively, the ion beam can be gradually decelerated before injection into an ion trap. This trap can then be filled with buffer gas, to slow the ions down to thermal temperatures, and/or dynamically caught by applying time-dependent potentials to the trap electrodes [81,82].

The production rates of different radio-isotopes vary strongly depending on the chosen reaction, target, primary beam intensity and energy, and other details of the RIB extraction process. Figure 3 shows typical yields which can be delivered to the user, of Ca and Sr, both alkaline-earth elements, at the Isotope Separator On-Line facility (ISOLDE) in CERN, Switzerland, and at the Ion Guide Isotope Separator On-line (IGISOL) facility in Jyväskylä, Finland. In the case of the ISOLDE facility, this figure presents measured yields, with a uranium carbide target (Ca: $A > 46$; Sr: $A > 87$), a Ti target (Ca: $A < 46$) a Nb foil target (Sr with $A < 88$). The data for IGISOL represent empirically scaled estimates based on TALYS [83] cross sections for Ca (Ca: protons or deuterons impinging on naturally abundant Ca targets; Sr: protons on enriched Sr targets), or scaled based on empirical fission cross-section data for Sr. Isotopes with a half-life below 1 s are shown with open symbols. A correction accounting for the half-lives and the extraction time from the target-ion guide system was taken into account, which only affects the most neutron-rich Sr isotopes.

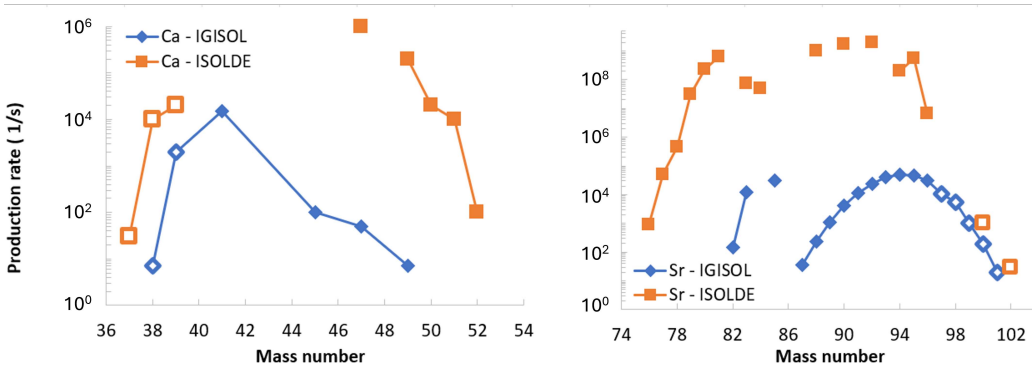

Figure 3. The calculated (IGISOL) and measured (ISOLDE) production yields of isotopes in the calcium (left) and strontium (right) isotopic chains. In all cases, the beam–target combination which maximized the production rate was chosen. Open symbols indicate isotopes with a half-life below 1 s. More details can be found in the text.

While there can be large differences in the production yields between different facilities, production rates (significantly) above 10 ions per second can be achieved for a long isotopic chain at either facility. If trap loading efficiencies of ten percent or more can be achieved, these production rates are sufficiently high to enable loading at least a few ions into the trap in one filling cycle, sufficient for a precision measurement. With a one-second half-life, experimental linewidths in the order of 1 Hz are, in principle, possible, assuming the trapping and preparation steps can be performed suitably fast; this thus does not impose strong limitations to the final precision. Shorter half-lives may, however, lead to decay during, e.g., the cooling or preparation stage. One clear technical requirement of a future radioactive trapped-ion experiment is thus to optimize the time it takes to fully prepare

the ion for a measurement, to prevent these losses. Finally, it is interesting to note that there are still many cases left unmeasured with half-lives of many hours, days, or even years. Thanks to the non-destructive nature of the measurement techniques outlined above, experiments could be performed in a 'parasitic mode', in parallel with other experiments, as only occasional filling of the ion trap would be required. This is advantageous, given the strong competition for access to RIB laboratories.

The general arguments provided in the preceding paragraphs are supported by the work presented in refs. [7–9]. In this work, after thermalization in a gas-filled stopper cell, ions were guided into a buffer gas-filled linear ion trap, which cooled them close to room temperature. Then, the gas flow was stopped so the ions could be further laser-cooled. This approach offered good trapping efficiencies, and was sufficiently fast to study 11Be, with a half-life of 13.76 s and a delivered beam intensity of only a few 100 ions/s. A similar timescale in the order of a few seconds was demonstrated as well using sympathetic cooling of long-lived Th isotopes, produced with an external ion source [82], albeit not in an 'online' experiment at an RIB facility.

In addition to considerations of lifetime and production rate, the purity of the ion beam should also be carefully considered. This purity can vary widely depending on the beam–target combination and primary beam energy, but in all cases, the beam will contain significant fractions of other isobars. When pushing far from stability, the production of these isobars can be orders of magnitude more efficient than the production of the isotopes of interest. Beam purification prior to injection is thus highly desirable. An interesting option could be to use a Penning trap, both for hyperfine structure spectroscopy and for mass purification. Alternatively, a multi-reflection time-of-flight (MR-TOF) mass spectrometer [84–90] located upstream of the spectroscopy trap may offer the most convenient solution.

4. Conclusions

This article provided an up-to-date summary of precision measurements of nuclear g-factors and hyperfine constants performed using ion traps. These atomic constants can be used to extract nuclear physics observables, e.g., hyperfine anomalies or higher-order nuclear moments. However, as these measurements are predominantly performed on stable isotopes only, extracting insight into nuclear structure physics is challenging. This article therefore also aimed to show that precision measurements on shorter-lived species, produced in accelerator-based facilities, are technically feasible. Indeed, trapped-ion precision spectroscopy techniques only require small numbers of ions (typically only one trapped ion at a given time) and can take place on rather fast timescales. Combined with the high production rates of many radioactive isotopes and the ability of radioactive ion beam facilities to provide these ions at room temperature, extended measurements on long isotopic chains form a promising avenue for new nuclear physics studies. Finally, the examples provided in this article show that, while alkaline-earth-like atoms are most conveniently studied with high precision, precision measurements can also be performed on more complex atoms. All of this combined implies a bright future for nuclear-physics-motivated studies using precision spectroscopy of radioactive trapped ions.

Funding: This research was funded by the FWO project G0A0723N and the FWO Odysseus project G0F7321N.

Data Availability Statement: The original contributions presented in the study are included in the article, further inquiries can be directed to the corresponding author.

Conflicts of Interest: The authors declare no conflicts of interest.

References

1. Savard, G.; Werth, G. Precision nuclear measurements with ion traps. *Annu. Rev. Nucl. Part. Sci.* **2000**, *50*, 119–152. [CrossRef]
2. Door, M.; Yeh, C.H.; Heinz, M.; Kirk, F.; Lyu, C.; Miyagi, T.; Berengut, J.C.; Bieroń, J.; Blaum, K.; Dreissen, L.S.; et al. Search for new bosons with ytterbium isotope shifts. *arXiv* **2024**, arXiv:2403.07792.

3. Knab, H.; Schupp, M.; Werth, G. Precision spectroscopy on trapped radioactive ions: Ground-state hyperfine splittings of $^{133}Ba^{+}$ and $^{131}Ba^{+}$. *Europhys. Lett.* **1987**, *4*, 1361. [CrossRef]
4. Enders, K.; Stachowska, E.; Marx, G.; Zölch, C.; Georg, U.; Dembczynski, J.; Werth, G.; Collaboration, I. Ground-state hyperfine-structure measurements of unstable Eu^{+} isotopes in a Paul ion trap. *Phys. Rev. A* **1997**, *56*, 265. [CrossRef]
5. Thielking, J.; Okhapkin, M.V.; Głowacki, P.; Meier, D.M.; von der Wense, L.; Seiferle, B.; Düllmann, C.E.; Thirolf, P.G.; Peik, E. Laser spectroscopic characterization of the nuclear-clock isomer 229mTh. *Nature* **2018**, *556*, 321–325. [CrossRef]
6. Christensen, J.E.; Hucul, D.; Campbell, W.C.; Hudson, E.R. High-fidelity manipulation of a qubit enabled by a manufactured nucleus. *Npj Quantum Inf.* **2020**, *6*, 35. [CrossRef]
7. Nakamura, T.; Wada, M.; Okada, K.; Takamine, A.; Ishida, Y.; Yamazaki, Y.; Kambara, T.; Kanai, Y.; Kojima, T.; Nakai, Y.; et al. Laser spectroscopy of $^{7,10}Be^{+}$ in an online ion trap. *Phys. Rev. A* **2006**, *74*, 052503. [CrossRef]
8. Okada, K.; Wada, M.; Nakamura, T.; Takamine, A.; Lioubimov, V.; Schury, P.; Ishida, Y.; Sonoda, T.; Ogawa, M.; Yamazaki, Y.; et al. Precision Measurement of the Hyperfine Structure of Laser-Cooled Radioactive $^{7}Be^{+}$ Ions Produced by Projectile Fragmentation. *Phys. Rev. Lett.* **2008**, *101*, 212502. [CrossRef] [PubMed]
9. Takamine, A.; Wada, M.; Okada, K.; Sonoda, T.; Schury, P.; Nakamura, T.; Kanai, Y.; Kubo, T.; Katayama, I.; Ohtani, S.; et al. Hyperfine Structure Constant of the Neutron Halo Nucleus $^{11}Be^{+}$. *Phys. Rev. Lett.* **2014**, *112*, 162502. [CrossRef]
10. Versolato, O.; Giri, G.; Van den Berg, J.; Böll, O.; Dammalapati, U.; Van Der Hoek, D.; Hoekstra, S.; Jungmann, K.; Kruithof, W.; Müller, S.; et al. Hyperfine structure of the 6d $^{2}D_{3/2}$ level in trapped short-lived $^{211,209}Ra^{+}$ ions. *Phys. Lett. A* **2011**, *375*, 3130–3133. [CrossRef]
11. Thompson, R. Spectroscopy of trapped ions. *Adv. At. Mol. Opt. Phys.* **1993**, *31*, 63–136.
12. Werth, G. Optical spectroscopy in ion traps. *Eur. Phys. J. D* **2007**, *45*, 121–124. [CrossRef]
13. Werth, G.; Gheorghe, V.N.; Major, F.G.; Werth, G.; Gheorghe, V.N.; Major, F.G. Optical Spectroscopy. In *Charged Particle Traps II: Applications*; Springer: Berlin/Heidelberg, Germany, 2009; pp. 129–159.
14. Wang, L.B.; Mueller, P.; Bailey, K.; Drake, G.; Greene, J.; Henderson, D.; Holt, R.; Janssens, R.; Jiang, C.; Lu, Z.T.; et al. Laser Spectroscopic Determination of the ^{6}He Nuclear Charge Radius. *Phys. Rev. Lett.* **2004**, *93*, 142501. [CrossRef]
15. Mueller, P.; Sulai, I.; Villari, A.; Alcántara-Núñez, J.; Alves-Condé, R.; Bailey, K.; Drake, G.; Dubois, M.; Eléon, C.; Gaubert, G.; et al. Nuclear Charge Radius of ^{8}He. *Phys. Rev. Lett.* **2007**, *99*, 252501. [CrossRef]
16. Zhang, J.; Tandecki, M.; Collister, R.; Aubin, S.; Behr, J.; Gomez, E.; Gwinner, G.; Orozco, L.; Pearson, M.; Sprouse, G.; et al. Hyperfine anomalies in Fr: boundaries of the spherical single particle model. *Phys. Rev. Lett.* **2015**, *115*, 042501. [CrossRef]
17. Kimura, N.; Kono, Y.; Pipatpakorn, P.; Soutome, K.; Numadate, N.; Kuma, S.; Azuma, T.; Nakamura, N. Hyperfine-structure-resolved laser spectroscopy of many-electron highly charged ions. *Commun. Phys.* **2023**, *6*, 8. [CrossRef]
18. Hur, J.; Aude Craik, D.P.; Counts, I.; Knyazev, E.; Caldwell, L.; Leung, C.; Pandey, S.; Berengut, J.C.; Geddes, A.; Nazarewicz, W.; et al. Evidence of two-source King plot nonlinearity in spectroscopic search for new Boson. *Phys. Rev. Lett.* **2022**, *128*, 163201. [CrossRef] [PubMed]
19. Reinhard, P.G.; Nazarewicz, W.; Ruiz, R.G. Beyond the charge radius: The information content of the fourth radial moment. *Phys. Rev. C* **2020**, *101*, 021301. [CrossRef]
20. Schwartz, C. Theory of Hyperfine Structure. *Phys. Rev.* **1955**, *97*, 380–395. [CrossRef]
21. De Groote, R.; Kujanpää, S.; Koszorús, Á.; Li, J.; Moore, I. Magnetic octupole moment of ^{173}Yb using collinear laser spectroscopy. *Phys. Rev. A* **2021**, *103*, 032826. [CrossRef]
22. Gustavsson, M.G.; Mårtensson-Pendrill, A.M. Four decades of hyperfine anomalies. In *Advances in Quantum Chemistry*; Elsevier: Amsterdam, The Netherlands, 1998; Volume 30, pp. 343–360.
23. Persson, J.R. Table of hyperfine anomaly in atomic systems. *At. Data Nucl. Data Tables* **2013**, *99*, 62–68. [CrossRef]
24. Yang, X.; Wang, S.; Wilkins, S.; Ruiz, R.G. Laser spectroscopy for the study of exotic nuclei. *Prog. Part. Nucl. Phys.* **2023**, *129*, 104005. [CrossRef]
25. Neyens, G. Nuclear magnetic and quadrupole moments for nuclear structure research on exotic nuclei. *Rep. Prog. Phys.* **2003**, *66*, 633. [CrossRef]
26. de Groote, R.P.; Neyens, G. Spins and Electromagnetic Moments of Nuclei. In *Handbook of Nuclear Physics*; Springer: Berlin/Heidelberg, Germany, 2022; pp. 1–36.
27. Becker, O.; Enders, K.; Werth, G.; Dembczynski, J. Hyperfine-structure measurements of the $^{151,153}Eu^{+}$ ground state. *Phys. Rev. A* **1993**, *48*, 3546. [CrossRef]
28. Xiao, D.; Li, J.; Campbell, W.C.; Dellaert, T.; McMillin, P.; Ransford, A.; Roman, C.; Derevianko, A. Hyperfine structure of Yb^{+} 173: Toward resolving the Yb 173 nuclear-octupole-moment puzzle. *Phys. Rev. A* **2020**, *102*, 022810. [CrossRef]
29. Major, F.G.; Gheorghe, V.N.; Werth, G. *Charged Particle Traps: Physics and Techniques of Charged Particle Field Confinement*; Springer Science & Business Media: Berlin/Heidelberg, Germany, 2005; Volume 37.
30. Ghosh, P.K. *Ion Traps*; Oxford University Press: Oxford, UK, 1995.
31. Blaum, K.; Novikov, Y.N.; Werth, G. Penning traps as a versatile tool for precise experiments in fundamental physics. *Contemp. Phys.* **2010**, *51*, 149–175. [CrossRef]
32. Dilling, J.; Blaum, K.; Brodeur, M.; Eliseev, S. Penning-trap mass measurements in atomic and nuclear physics. *Annu. Rev. Nucl. Part. Sci.* **2018**, *68*, 45–74. [CrossRef]

33. Nagourney, W.; Sandberg, J.; Dehmelt, H. Shelved optical electron amplifier: Observation of quantum jumps. *Phys. Rev. Lett.* **1986**, *56*, 2797. [CrossRef]
34. Zoller, P.; Marte, M.; Walls, D. Quantum jumps in atomic systems. *Phys. Rev. A* **1987**, *35*, 198. [CrossRef]
35. Schmidt, P.O.; Rosenband, T.; Langer, C.; Itano, W.M.; Bergquist, J.C.; Wineland, D.J. Spectroscopy using quantum logic. *Science* **2005**, *309*, 749–752. [CrossRef]
36. Hume, D.B.; Rosenband, T.; Wineland, D.J. High-Fidelity Adaptive Qubit Detection through Repetitive Quantum Nondemolition Measurements. *Phys. Rev. Lett.* **2007**, *99*, 120502. [CrossRef]
37. Lewty, N.C.; Chuah, B.L.; Cazan, R.; Sahoo, B.K.; Barrett, M.D. Spectroscopy on a single trapped $^{137}Ba^{+}$ ion for nuclear magnetic octupole moment determination. *Opt. Express* **2012**, *20*, 21379–21384. [CrossRef] [PubMed]
38. Li, J.; Gaigalas, G.; Bieroń, J.; Ekman, J.; Jönsson, P.; Godefroid, M.; Froese Fischer, C. Re-evaluation of the nuclear magnetic octupole moment of 209Bi. *Atoms* **2022**, *10*, 132. [CrossRef]
39. Rabi, I.I.; Millman, S.; Kusch, P.; Zacharias, J.R. The molecular beam resonance method for measuring nuclear magnetic moments. the magnetic moments of $_3Li^6$, $_3Li^6$ and $_9F^{19}$. *Phys. Rev.* **1939**, *55*, 526. [CrossRef]
40. Lewty, N.C.; Chuah, B.L.; Cazan, R.; Barrett, M.D.; Sahoo, B.K. Experimental determination of the nuclear magnetic octupole moment of $^{137}Ba^{+}$ ion. *Phys. Rev. A* **2013**, *88*, 012518. [CrossRef]
41. Hoffman, M.R. Observation of the Nuclear Magnetic Octupole Moment of 137Ba+. Ph.D. Thesis, University of Washington, Seattle, WA USA, 2014.
42. Itano, W.M.; Bergquist, J.C.; Bollinger, J.J.; Wineland, D.J. Cooling methods in ion traps. *Phys. Scr.* **1995**, *1995*, 106. [CrossRef]
43. Karr, J.P. Precision measurements with non-laser-cooled trapped ions. *J. Phys. At. Mol. Opt. Phys.* **2009**, *42*, 154018. [CrossRef]
44. Enders, K.; Stachowska, E.; Marx, G.; Zölch, C.; Revalde, G.; Dembczynski, J.; Werth, G. Hyperfine structure measurements in the 7 S 3 metastable finestructure level in stable and unstable Eu+ isotopes. *Z. Für Phys. D At. Mol. Clust.* **1997**, *42*, 171–175.
45. Eschner, J.; Morigi, G.; Schmidt-Kaler, F.; Blatt, R. Laser cooling of trapped ions. *JOSA B* **2003**, *20*, 1003–1015. [CrossRef]
46. Peik, E.; Abel, J.; Becker, T.; von Zanthier, J.; Walther, H. Sideband cooling of ions in radio-frequency traps. *Phys. Rev. A* **1999**, *60*, 439–449. [CrossRef]
47. Monroe, C.; Meekhof, D.M.; King, B.E.; Jefferts, S.R.; Itano, W.M.; Wineland, D.J.; Gould, P. Resolved-Sideband Raman Cooling of a Bound Atom to the 3D Zero-Point Energy. *Phys. Rev. Lett.* **1995**, *75*, 4011–4014. [CrossRef]
48. Morigi, G.; Eschner, J.; Keitel, C.H. Ground State Laser Cooling Using Electromagnetically Induced Transparency. *Phys. Rev. Lett.* **2000**, *85*, 4458–4461. [CrossRef] [PubMed]
49. Roos, C.F.; Leibfried, D.; Mundt, A.; Schmidt-Kaler, F.; Eschner, J.; Blatt, R. Experimental Demonstration of Ground State Laser Cooling with Electromagnetically Induced Transparency. *Phys. Rev. Lett.* **2000**, *85*, 5547–5550. [CrossRef] [PubMed]
50. Larson, D.J.; Bergquist, J.C.; Bollinger, J.J.; Itano, W.M.; Wineland, D.J. Sympathetic cooling of trapped ions: A laser-cooled two-species nonneutral ion plasma. *Phys. Rev. Lett.* **1986**, *57*, 70–73. [CrossRef] [PubMed]
51. Persson, J. Extraction of hyperfine anomalies without precise values of the nuclear magnetic dipole moment. *Eur. Phys. J.-Hadron. Nucl.* **1998**, *2*, 3–4. [CrossRef]
52. Schmidt, T. Über die magnetischen Momente der Atomkerne. *Z. Für Phys.* **1937**, *106*, 358–361. [CrossRef]
53. Angeli, I.; Marinova, K.P. Table of experimental nuclear ground state charge radii: An update. *At. Data Nucl. Data Tables* **2013**, *99*, 69–95. [CrossRef]
54. Wineland, D.; Itano, W.M.; Van Dyck Jr, R. High-Resolution Spectroscopy of Stored Ions. *Adv. At. Mol. Phys.* **1983**, *19*, 135–186.
55. Arbes, F.; Benzing, M.; Gudjons, T.; Kurth, F.; Werth, G. Precise determination of the ground state hyperfine structure splitting of ^{43}Ca II. *Z. Für Phys. D At. Mol. Clust.* **1994**, *31*, 27–30. [CrossRef]
56. Nakamura, T.; Wada, M.; Okada, K.; Katayama, I.; Ohtani, S.; Schuessler, H. Precision spectroscopy of the Zeeman splittings of the $^9Be^+$ $2^2S_{1/2}$ hyperfine structure for nuclear structure studies. *Opt. Commun.* **2002**, *205*, 329–336. [CrossRef]
57. Itano, W.M.; Wineland, D. Precision measurement of the ground-state hyperfine constant of $^{25}Mg^{+}$. *Phys. Rev. A* **1981**, *24*, 1364. [CrossRef]
58. Rosenband, T.; Schmidt, P.O.; Hume, D.B.; Itano, W.M.; Fortier, T.M.; Stalnaker, J.E.; Kim, K.; Diddams, S.A.; Koelemeij, J.C.J.; Bergquist, J.C.; et al. Observation of the $^1S_0 \rightarrow ^3P_0$ Clock Transition in $^{27}Al^{+}$. *Phys. Rev. Lett.* **2007**, *98*, 220801. [CrossRef]
59. Hanley, R.K.; Allcock, D.T.C.; Harty, T.P.; Sepiol, M.A.; Lucas, D.M. Precision measurement of the $^{43}Ca^{+}$ nuclear magnetic moment. *Phys. Rev. A* **2021**, *104*, 052804. [CrossRef]
60. Marx, G.; Tommaseo, G.; Werth, G. Precise g_J-and g_I-factor measurements of Ba^{+} isotopes. *Eur. Phys. J. -At. Mol. Opt. Plasma Phys.* **1998**, *4*, 279–284.
61. Trapp, S.; Tommaseo, G.; Revalde, G.; Stachowska, E.; Szawiola, G.; Werth, G. Ion trap nuclear resonance on $^{151}Eu^{+}$. *Eur. Phys. J. -At. Mol. Opt. Plasma Phys.* **2003**, *26*, 237–244.
62. Schuessler, H.A.; Fortson, E.N.; Dehmelt, H.G. Hyperfine Structure of the Ground State of $^3He^{+}$ by the Ion-Storage Exchange-Collision Technique. *Phys. Rev.* **1969**, *187*, 5–38. [CrossRef]
63. Shiga, N.; Itano, W.M.; Bollinger, J.J. Diamagnetic correction to the $^9Be^{+}$ ground-state hyperfine constant. *Phys. Rev. A* **2011**, *84*, 012510. [CrossRef]
64. Xu, Z.; Deng, K.; Che, H.; Yuan, W.; Zhang, J.; Lu, Z. Precision measurement of the $^{25}Mg^{+}$ ground-state hyperfine constant. *Phys. Rev. A* **2017**, *96*, 052507. [CrossRef]
65. Trainham, R.; Jopson, R.; Larson, D.J. Measurement of the hyperfine structure of 33 S-. *Phys. Rev. A* **1989**, *39*, 3223. [CrossRef]

66. Sunaoshi, H.; Fukashiro, Y.; Furukawa, M.; Yamauchi, M.; Hayashibe, S.; Shinozuka, T.; Fujioka, M.; Satoh, I.; Wada, M.; Matsuki, S. A precision measurement of the hyperfine structure of $^{87}Sr^{+}$. *Hyperfine Interact.* **1993**, *78*, 241–245. [CrossRef]
67. Zhang, J.W.; Wang, Z.B.; Wang, S.G.; Miao, K.; Wang, B.; Wang, L.J. High-resolution laser microwave double-resonance spectroscopy of hyperfine splitting of trapped $^{113}Cd^{+}$ and $^{111}Cd^{+}$ ions. *Phys. Rev. A* **2012**, *86*, 022523. [CrossRef]
68. Tanaka, U.; Imajo, H.; Hayasaka, K.; Ohmukai, R.; Watanabe, M.; Urabe, S. Determination of the ground-state hyperfine splitting of trapped $^{113}Cd^{+}$ ions. *Phys. Rev. A* **1996**, *53*, 3982–3985. [CrossRef] [PubMed]
69. Jelenković, B.M.; Chung, S.; Prestage, J.D.; Maleki, L. High-resolution microwave-optical double-resonance spectroscopy of hyperfine splitting of trapped $^{113}Cd^{+}$ ions. *Phys. Rev. A* **2006**, *74*, 022505. [CrossRef]
70. Miao, S.N.; Zhang, J.W.; Qin, H.R.; Xin, N.C.; Han, J.Z.; Wang, L.J. Precision determination of the ground-state hyperfine splitting of trapped $^{113}Cd+$ ions. *Opt. Lett.* **2021**, *46*, 5882–5885. [CrossRef]
71. Becker, W.; Werth, G. Precise determination of the ground state hyperfine splitting of $^{135}Ba^{+}$. *Z. Für Phys. Atoms Nucl.* **1983**, *311*, 41–47. [CrossRef]
72. Blatt, R.; Werth, G. Precision determination of the ground-state hyperfine splitting in $^{137}Ba^{+}$ using the ion-storage technique. *Phys. Rev. A* **1982**, *25*, 1476–1482. [CrossRef]
73. Fisk, P.T.; Sellars, M.J.; Lawn, M.A.; Coles, G. Accurate measurement of the 12.6 GHz "clock" transition in trapped $^{171}Yb^{+}$ ions. *IEEE Trans. Ultrason. Ferroelectr. Freq. Control.* **1997**, *44*, 344–354. [CrossRef]
74. Tamm, C.; Schnier, D.; Bauch, A. Radio-frequency laser double-resonance spectroscopy of trapped ^{171}Yb ions and determination of line shifts of the ground-state hyperfine resonance. *Appl. Phys. B* **1995**, *60*, 19–29. [CrossRef]
75. Phoonthong, P.; Mizuno, M.; Kido, K.; Shiga, N. Determination of the absolute microwave frequency of laser-cooled $^{171}Yb^{+}$. *Appl. Phys. B* **2014**, *117*, 673–680. [CrossRef]
76. Münch, A.; Berkler, M.; Gerz, C.; Wilsdorf, D.; Werth, G. Precise ground-state hyperfine splitting in ^{171}Yb II. *Phys. Rev. A* **1987**, *35*, 4147. [CrossRef]
77. McGuire, M.D.; Petsch, R.; Werth, G. Precision determination of the ground-state hyperfine separation in $^{199}Hg^{+}$ using the ion-storage technique. *Phys. Rev. A* **1978**, *17*, 1999–2004. [CrossRef]
78. Liu, H.; Yang, Y.N.; He, Y.H.; Li, H.X.; Chen, Y.H.; She, L.; Li, J.M. Microwave-Optical Double-Resonance Spectroscopy Experiment of $^{199}Hg^{+}$ Ground State Hyperfine Splitting in a Linear Ion Trap. *Chin. Phys. Lett.* **2014**, *31*, 063201. [CrossRef]
79. Berkeland, D.J.; Miller, J.D.; Bergquist, J.C.; Itano, W.M.; Wineland, D.J. Laser-Cooled Mercury Ion Frequency Standard. *Phys. Rev. Lett.* **1998**, *80*, 2089–2092. [CrossRef]
80. Feng, X.; Li, G.Z.; Werth, G. High-precision hyperfine spectroscopy in M1-M1 double-resonance transitions on trapped $^{207}Pb^{+}$. *Phys. Rev. A* **1992**, *46*, 2959–2961. [CrossRef] [PubMed]
81. Groot-Berning, K.; Stopp, F.; Jacob, G.; Budker, D.; Haas, R.; Renisch, D.; Runke, J.; Thörle-Pospiech, P.; Düllmann, C.E.; Schmidt-Kaler, F. Trapping and sympathetic cooling of single thorium ions for spectroscopy. *Phys. Rev. A* **2019**, *99*, 023420. [CrossRef]
82. Zitzer, G.; Tiedau, J.; Okhapkin, M.; Zhang, K.; Mokry, C.; Runke, J.; Düllmann, C.E.; Peik, E. Sympathetic cooling of trapped Th 3+ alpha-recoil ions for laser spectroscopy. *Phys. Rev. A* **2024**, *109*, 033116. [CrossRef]
83. Koning, A.; Hilaire, S.; Goriely, S. TALYS: modeling of nuclear reactions. *Eur. Phys. J. A* **2023**, *59*, 131. [CrossRef]
84. Ishida, Y.; Wada, M.; Wollnik, H. A multi-reflection time-of-flight mass spectrometer for mass measurements of short-lived nuclei. *Nucl. Instruments Methods Phys. Res. Sect. Beam Interact. Mater. Atoms* **2005**, *241*, 983–985. [CrossRef]
85. Wolf, R.; Wienholtz, F.; Atanasov, D.; Beck, D.; Blaum, K.; Borgmann, C.; Herfurth, F.; Kowalska, M.; Kreim, S.; Litvinov, Y.A.; et al. ISOLTRAP's multi-reflection time-of-flight mass separator/spectrometer. *Int. J. Mass Spectrom.* **2013**, *349*, 123–133. [CrossRef]
86. Plaß, W.R.; Dickel, T.; Scheidenberger, C. Multiple-reflection time-of-flight mass spectrometry. *Int. J. Mass Spectrom.* **2013**, *349*, 134–144. [CrossRef]
87. Jesch, C.; Dickel, T.; Plaß, W.R.; Short, D.; Andres, S.A.S.; Dilling, J.; Geissel, H.; Greiner, F.; Lang, J.; Leach, K.G.; et al. The MR-TOF-MS isobar separator for the TITAN facility at TRIUMF. In Proceedings of the TCP 2014: Proceedings of the 6th International Conference on Trapped Charged Particles and Fundamental Physics, Takamatsu, Japan, 1–5 December 2014; Springer: Berlin/Heidelberg, Germany, 2017; pp. 175–184.
88. Hirsh, T.Y.; Paul, N.; Burkey, M.; Aprahamian, A.; Buchinger, F.; Caldwell, S.; Clark, J.A.; Levand, A.F.; Ying, L.L.; Marley, S.T.; et al. First operation and mass separation with the CARIBU MR-TOF. *Nucl. Instrum. Methods Phys. Res. Sect. Beam Interact. Mater. Atoms* **2016**, *376*, 229–232. [CrossRef]
89. Chauveau, P.; Delahaye, P.; De France, G.; El Abir, S.; Lory, J.; Merrer, Y.; Rosenbusch, M.; Schweikhard, L.; Wolf, R. PILGRIM, a multi-reflection time-of-flight mass spectrometer for Spiral2-S3 at GANIL. *Nucl. Instrum. Methods Phys. Res. Sect. Beam Interact. Mater. Atoms* **2016**, *376*, 211–215. [CrossRef]
90. Virtanen, V. Offline Commissioning of the Multi-Reflection Time-of-Flight Mass Separator at JYFLTRAP. Master's Thesis, University of Jyväskylä, Jyväskylä, Finland, 2019.